# Neuronal leak within recurrent neuronal networks prevents the generation of high frequency spurious signals

Udaya B. Rongala[1], Jonas M.D. Enander[1], Matthias Kohler[2], Henrik Jörntell[1]

[1]Department of Experimental Medical Science, Faculty of Medicine, Lund University, Lund, Sweden

[2]Department of Informatics, Technical University of Munich, 85748 Garching, Germany

## Abstract

Elements of recurrent excitatory synaptic loops are present within sensorimotor control loops in the brain. Such positive feedback loops can cause self-amplification, which is potentially dangerous for the brain (as in epilepsy) or which may cause disruptive effects on of the information passed within the neuronal circuitry. Here we introduce a simplified non-spiking neuron model, whose output accurately reflects summated synaptic inputs, with which we performed simulations of highly connected networks composed of excitatory and inhibitory neurons in equal proportions. The neuron model could be optionally equipped with a dynamic leak, i.e. dynamic short-circuit to the resting membrane potential, equivalent to a membrane time constant. Synaptic weights were randomly assigned across the network according to a range of different types and ranges of distribution. Networks were provided with random and semi-structured sensory inputs and we studied the spread of activity through the network. We find that in neurons without dynamic leak, recurrent networks produced high frequency noise components that were not present in the input signal, across all synaptic weight distributions. The addition of dynamic leak consistently removed such high frequency noise. Conduction delays between neurons, when explicitly included, tended to worsen the high frequency noise, which was rescued by dynamic leak also in this case. Our findings suggest that neuronal dynamic short circuit of voltage deviations towards the resting potential serve the beneficial function of protecting recurrent neuronal circuitry from inducing itself into spurious high frequency signal generation, thereby permitting the brain to utilize this architectural circuitry component.

# Introduction

Many neuronal networks within sensorimotor brain structures contain elements of recurrent excitatory synaptic connections. Examples include the neocortical circuitry (Binzegger et al., 2004; Kar & DiCarlo, 2020; Papale & Hooks, 2018; Yamawaki et al., 2014), thalamo-cortical loops (Hooks et al., 2013; Phillips et al., 2019), and cerebellar-brainstem loops (Allen & Tsukahara, 1974). This type of connectivity poses a risk of the networks entering states of self-amplifying positive feedback loops. On the other hand, all of the above networks contain a prominent component of inhibitory neurons that could dampen the risk of the network entering such positive feedback loops.

Here we wanted to test the conditions under which a generic neuronal network would tend to fall into such positive feedback loops, and possible factors that could rescue the network from falling into such states. We aimed to test these issues in a model neuronal network with as few constraints as possible, while still preserving essential neuronal signalling features. We therefore introduce a non-spiking, non-conductance based, neuron model in which synaptic inputs from other neurons are weighted values of the activity of that neuron and where inhibitory neurons differ from excitatory neurons only by having negative synaptic weights on other neurons. We applied this neuron model to simulate fully connected, recurrent two layer neuronal networks with equal numbers of excitatory and inhibitory neurons. The input layer received varied, but internally correlated, information and by default it consisted of five excitatory and five inhibitory neurons that were fully interconnected with random weights. The excitatory neurons provided the sole input to the output layer, by default composed of four excitatory neurons and four inhibitory interneurons, again fully interconnected with random weights. The excitatory neurons of the output layer projected back to all neurons of the input layer, thus forming the recurrent component of the network. We found that this type of network structure apparently inevitably leads to reverberant, high-frequency transient signals, which was not present in the input data and therefore degraded the faithfulness of the neuronal signal representation of a given afferent input to the recurrent network.

# Methods

## Neuron Model

*Linear summation neuron model (LIS)*:

The neuron model implemented for this study was a normalized linear summation model with an additional leak component. Neuron activity without leak ($A$) was given by the total weighted activity ($w * a$) across all individual synapses ($i$) and normalized with a protection leak constant ($l$). The protection leak is equivalent to the number of static leak channels in a neuron, and the impact of synaptic activation in the neuron depends on the conductance of the synaptically operated channels relative to this static leak. Hence, in our LIS model, the value of the protection leak constant is based on the number of synapses provided to that given neuron. Furthermore, the neuron activity with leak ($A_L$) is given by the linear summation model with an additional leak time constant ($k$). The neuron activity of this model is given by following equations,

$$A = \left( \frac{\sum(w_i * a_i)}{l + \sum|w_i * a_i|} \right)$$

$$\dot{A}_L = (-A_L + A)/k$$

*Izhikevich neuron model (IZ)*:

For the Izhikevich neuron model (Izhikevich, 2003), the membrane potential ($v$) and the adaptation variable ($u$) were updated via the following nonlinear differential equations discretized using Euler's method

$$\dot{v} = Av^2 + Bv + C - u + \frac{I_{input}}{C}$$
$$\dot{u} = a(bv - u)$$

When the membrane potential reached the spike depolarization threshold of 30 $mV$, one spike was produced followed by a reset:

$$if\ v \geq 30\ mV, then \begin{cases} v \leftarrow c \\ u \leftarrow u + d \end{cases}$$

The $A, B, C$ parameters and the spiking threshold were the standard ones of the Izhikevich artificial neuron model, whereas the parameters $a, b, c\ and\ d$ were selected (*Table 1*) to allow a regular spiking behavior.

## Network Connectivity

Our network was a two-layer fully connected neuronal network architecture, that comprised both inhibitory interneurons (interneurons, $IN$) and excitatory neurons (neurons, $N$) (Figure 3A). The network architecture is defined based on the following four rules (*a*) The inputs are projected as excitatory synapses only on the excitatory neurons and the inhibitory interneurons in layer 1. (*b*) All the excitatory neurons in layer 1 and 2 are connected bi-directionally. (*c*) The excitatory neurons in both layers make excitatory

synaptic connections on the interneurons in both layers. (*d*) The interneurons make inhibitory synaptic connections onto all the neurons and interneurons in both layer 1 and 2. A "$5 \times 4$" network architecture (5 neurons/interneuron in layer 1 and 4 neurons/interneurons in layer 2) was considered throughout this work. In the analysis of Figure 5, where different network sizes were explored, we simply scaled up the number of neurons in each layer by the same numbers (Figure 5).

## Sensory Inputs

*Pseudo-random inputs:*

We generated pseudorandom spike times for several different frequencies (25, 50, 100 & 200 Hz, Figure 1A, 2) with uniform discrete distributions. We used an inbuilt MATLAB® function "*randi*" to generate these spike distributions. Further, these spikes were convoluted to time continuous activity given by the kernel (Mazzoni et al., 2008) of equation below,

$$a_{rnd} = \frac{\tau_1}{\tau_d - \tau_r} * \left[exp\left(-\frac{t - \tau_l - t^*}{\tau_d}\right) - exp\left(-\frac{t - \tau_l - t^*}{\tau_r}\right)\right]$$

Where, $t^*$ is the spike time, $\tau_d$ is the decay time (4 ms), $\tau_r$ is the rise time (12.5 ms) and $\tau_1$ is the constant to calculate ration between rise time and decay time (21.3 ms), and $\tau_l$ is the latency time which is zero in this case.

In order to validate the robustness, we have presented the neuron model with 50 repetitions of pseudorandom spike train. A random noise of $\pm$ 10 ms was added to individual spike times for each repetition (Figure 1C, D, E).

*Pseudo-real inputs:*

We also generated sensory data that contains intrinsic dynamic correlations between sensors (Figure 2, S3). To this end, a model plant was created with a link (L1) resting on a plane with a sliding constraint. A pair of antagonistic joints (J1, J2) was attached to L1. These joints were damped spring force generators, meaning that they could only pull, not push. The force output was controlled by changing the stiffness of the damped springs, which was randomly changed both with respect to amplitude and duration of change. The simulated sensors generated pseudo-realistic feedback of velocity (S1, S4), force (S2, S5) and length (S3, S6) (Figure 2A). A total of 500 seconds of simulated sensory feedback was generated. Then, each iteration cycle operated on one second of this simulated sensory feedback. The data was repeated five times during learning, for a total of 2500 iteration cycles.

## Synaptic Weights

The synaptic weights were randomly distributed across all the excitatory neurons and interneurons. The synaptic weight distributions used in this work were generated using normal distribution with mean ($\mu$) of 0.3 and cumulative variation ($cv$) of 20%, where sigma $(\sigma) = (cv/100) * \mu$.

The neuron model was tested with three different types of synaptic weight distributions (normal, lognormal and binary). Additionally, for normal and lognormal distributions the

mean of the distributions was varied between $0.1 - 0.5$ with a fixed $cv$ of 20%. For binary distributions, a probability (which was varied between 10% - 50%) of random synapses were set to high weight ($w = 1$), and the rest of synapses were set to zero weight (Figure 4A, B, C).

## Statistical Analysis

*Cross-correlation:*

The correlation index measure was used to compute similarity of the responses of the neuron models (Figure 1F, S1E) and to compute the intrinsic dynamic correlations between pseudo-real sensory inputs (Figure 2B). In Figure 2B, the boxplot illustrates the correlation measure between each sensory pair (S1-S6), for all the 2500 iterations (scatter plot, Figure 2B). The correlation between two signals was computed with an inbuilt MATLAB® function "*xcorr*" (with zero lag). A cross-correlation index measure of 1 denotes high similarity between two signals, whereas a measure towards 0 denotes high dissimilarity between the two given signals.

*Frequency analysis:*

We performed a continuous wavelet transform in order to define the frequency composition of a given signal, using an inbuilt MATLAB® function "*cwt*". In Figure 2C, the frequency analysis was performed on the sensory input signals for all 2500 iteration cycles. The maximum power computed for the sensory input signal, for each given frequency and iteration cycle, is reported in these plots (Figure 2C).

In Figure 3, the frequency analysis was performed on individual neuron and interneuron activity. Figure 3B shows the maximum power computed for the activity of a single neuron ($N_1$) across all frequencies and iteration cycles (the same analysis was made in Figure 3C, F and G). A similar frequency composition signal analysis was carried out in Figure S2, 4, 5 and 6, but here only the average power across 500 iteration cycles (Iteration cycle #500 - #1000) was reported.

# Results

## Neuron Model Derivation

We first describe the rationale for our Linear Summation (LIS) neuron model. In brief, the LIS neuron model is equivalent to H-H conductance-level models (Rongala et al., 2018), where the size of the time step (h) essentially equals the membrane time constant, but rids the model of the computational load of the associated differential equations.

The LIS neuron model can be derived from a Hodgkin-Huxley type of conductance based neuron model as follows. Consider the H-H neuron model where the reversal potentials of the inhibitory and excitatory synapses are set so that the neuron's membrane voltage is always in the interval [-1,1].

First, the H-H neuron model has both excitatory and inhibitory synaptic input currents, and a leak current, which all affect the membrane potential at a speed that is determined by the membrane capacitance:

$$C\frac{dv}{dt} = I_{leak} + I_{syn,exc} + I_{syn,inh}$$

Next, each synaptic current can be calculated as the sum of each synaptic weight times the activity in that synapses, for both excitatory and inhibitory synapses. The reversal potentials, which in biology are equivalent to the weighted Nernst potentials of each ion that is made permeable by synaptic activation, provide the bounds for the maximal synaptic response. Once the magnitude of a synaptic input is sufficiently large to drive the membrane potential to its reversal potential, any additional synaptic input gets scaled down towards zero. Then we arrive at the following equation for calculating the membrane potential:

$$\tau\frac{dv}{dt} = -V + (1-V)\sum w_j^+ V_j^+ + (1+V)\sum w_j V_j^-$$

For reasons of computational efficiency it is desirable to solve this differential equation with the Euler method and large time steps. This will, however, lead to numerical instability. For instance, if the neuron receives a high excitatory input it would overshoot the upper voltage boundary within the time step. In the next time step, the reversal potential would lead to a large undershoot of the voltage. In total this leads to oscillations, due to the numerical problem. The solution for this problem would be the application of higher order or implicit methods, at the cost of evaluating the differential equation many times per time or having to apply fixed point iterations. Alternatively one step of the backward Euler method can be applied directly to the differential equation to obtain a new system which has the same dynamics, but which can provide a numerically stable solution by the forward Euler method.

The approach of the backward Euler method to compute the voltage of the next time step is:

$$V_{t+1} = V_t + h\frac{1}{\tau}\left(-V_{t+1} + (1-V_{t+1})\sum w_j^+ V_j^+ + (1-V_{t+1})\sum w_j V_j^-\right)$$

where h is the time step.

Solving this equation for $V_{t+1}$ gives

$$V_{t+1} = \frac{V_t + \frac{h}{\tau}\sum w\, V}{1 + \frac{h}{\tau} + \frac{h}{\tau}\sum |w|\, V}$$

At first glance, dividing by the absolute of the synaptic weights times the synaptic input might look out of place, however this is a computational trick to ensure numerical stability of the neuron model and can also be directly motivated by biological considerations (see Methods).

The motivation for using a non-spiking neuron model is as follows: biological neurons spike and most neuronal network models include spiking as an essential feature. However, spike generation is an intrinsically stochastic process and as such it is associated with a variability that is hard to accurately capture in a model (Spanne et al., 2014). Previous systematic analyses of the input-output relationships across a range of neuron types in the central nervous system in vivo indicate that the spike output can be regarded as a probability density function (PDF) of the underlying membrane potential of the neuron (Spanne et al., 2014). This PDF is linear in the range between just above firing threshold and the saturation of the action potential generation mechanism (Spanne et al., 2014). Hence, neuronal input-output can be well approximated by the time-modulated membrane potential of the neuron, thereby by-passing the difficult step of calculating when spikes should be triggered.

## Comparison to Spiking Neuron Models

We first explored how the output activity of the LIS neuron model compared with that of a spiking neuron model in terms of information conveyed. We chose the Izhikevich (IZ) neuron model for this comparison, as this model was founded to mimic rich neuronal spiking behavior with computational efficiency (Izhikevich, 2003). Both neuron models (LIS & IZ) were provided with the same pseudo-random inputs (see Methods) from 5 different synapses (Figure 1B, random weight). The spikes generated by the IZ neuron model were convoluted (see Methods) to a time continuous signal (Figure 1E), in-order to compare it with the LIS neuron model output (Figure 1C, D).

The main difference between the LIS and the IZ neuron model responses was that the IZ neuron model tended to create a more dynamic output signal, despite that such dynamics was not present in the input signal (Figure 1B). With the LIS neuron model, the addition of dynamic leak created a behavior that was more similar to that of the spiking neuron, but still with substantially less information loss of the input signal (Figure 1C, F). A cross-correlation analysis between the neurons' input-output responses (Figure 1F) and between both the neuron models responses (Figure 1G) shows that, the activity of the both the neuron models (IZ & LIS) was relatively highly correlated (Figure 1G), whereas the differences found led to that the IZ neuron model was less faithfully reflecting the input signal than LIS neuron model (Figure 1F). Further, we compared both the outputs of the neuron models for different spike frequencies in the input. A high correlation between the input signals and the LIF neuron model output was consistent across the full range of input spike frequencies (Figure S2).

### Network Dynamics (with and without Neuronal Leak)

We further focused on the dynamic leak component in the neuron model. We investigated its effects on the dynamics of a fully connected neuronal network with both excitatory neurons and inhibitory interneurons (Figure 3A). This network was examined with and without the dynamic leak component of the LIS neuron model (for both neurons and interneuron). Time-continuous sensory input data (pseudo-real inputs, see Methods) was fed as excitatory input to the neurons and interneurons in the network for 2500 iteration cycles.

In networks of the neuron model without dynamic leak, there was an increase in the power across higher frequency components in the activities of each individual excitatory neuron and inhibitory interneuron (Figure 3B, C). This high frequency component was not present within the sensory input (Figure 2C). This high frequency component must therefore have been generated by and propagated within the network. Appearance of these high frequency components was associated with the appearance of transients in the neuron activity (Figure 3D, E). In contrast, in networks of the neuron model with the dynamic leak component (LIS with leak) the transients completely disappeared from the neuron/interneuron's activity (Figure 3 F -I).

This phenomenon of transients in the neuron activity was also observed with different synaptic weight distributions of the network (Figure 4). Different synaptic weight settings were randomly generated (five repetitions) Gaussian, log-normal and binary distributions that in each case was distributed across all neurons and interneurons of the network (Figure 4A, B, C). When the LIS neuron model was implemented without leak, high-frequency components appeared across all the synaptic weight distributions, for which at least a minimal amount of activity could be built up within the network (mu ≥ 0.3 for both gaussian and log-normal distributions, and p ≥ 30% for binary distribution) (Figure 4D). However, with addition of dynamic leak to LIS neuron model, these transients disappeared in all cases (Figure 4E).

We also explored if the size of the network could be a factor for the appearance of the high frequency components. We found that these high frequency components appeared regardless of network size and that in each case the network could be 'rescued' from the appearance of these components when the LIS neuron model was implemented with the dynamic leak (Figure 5). In addition, when we introduced conduction delays between all of the neurons the high frequency components could rise dramatically for delays shorter than 5 ms (Figure 6).

## Discussion

Here we found that recurrent networks of neurons without dynamic leak tend to generate spurious high-frequency components in the processed signal, which was not present in the external afferent input signal driving the network activity. We found that this phenomenon persisted across a range of network configurations, in terms of the synaptic weight distributions and network sizes. In all cases, we found that the phenomenon was effectively cancelled out by neuronal dynamic leak. As the dynamic leak as a consequence helped the

activity of the neurons to become more correlated with the input signal, we conclude that for the present neuronal network models, dynamic leak rescues the fully recurrent network from injecting high frequency noise components into the signal processed by the network.

The observed transients, or high-frequency signals, likely arose because of the derivation of the local signals caused by feed-forward inhibition of excitatory signals. Initial signal derivation is then likely amplified at each subsequent synaptic relay, and because of the recurrent structure of the network, these transient signals can never die out as long as the excitation level of the network is prevented from falling towards zero (in our case, sustained external afferent input to the network was what prevented this from happening). These transients continued to spread and tended to self-amplify over time, gradually diminishing the relative influence of the external sensory input on the internal network activity.

Interestingly, the addition of small delays, equivalent to local axon conduction times between neurons in the cortex for example, tended to amplify the transients. Due to the signal conversion process at the synapse, where an electrical signal (the action potential) is converted into a molecular signal in the presynaptic terminal and then back again to an electrical signal in the postsynaptic neuron, such delays are an inevitable limitation of biological systems. It is also a fact that neurons communicate signals between them using axons, which is another source of delay in biological neuronal networks. What our findings indicate is hence that this delay would tend to amplify spurious high-frequency signal generation. The neuronal dynamic leak helped alleviating also this component of spurious signal generation.

The dynamic leak tends to low-pass filter, hence delaying, or flattening, signals transmitted and is the likely mechanism 'rescuing' the network activity. Spikes in neurons have afterhyperpolarizations that make the neurons refractory to further signal transmission for narrow time windows. This aspect of neuronal signal processing would instead tend to high-pass signals, which would further worsen the tendency for self-amplifying transients. In real biological neuronal networks with recurrent connectivity structure, the dynamic leak would contribute to dampening also spike-induced, spurious high-frequency signal components, thus preserving faithfulness to the information in the original input signal.
What does spiking add anyway, in terms of brain functionality? Could be a limitation caused by the biological need for electrical signaling, which is required to send information large distances at highest possible speed, but comes with the trade-off of losing information. Spikes are noisy, hence neuronal redundancy could be the brain's solution to dealing with the noise that results. But in simulations a more efficient implementation would be to simply skip spikes.

The present findings suggest that the biological feature of neuronal dynamic leak, which causes the activity of the neuron to dissipate towards zero with a time constant, is an important functional feature that allows brain networks to fully utilize recurrent neuronal network architectures.

## References


Allen, G. I., & Tsukahara, N. (1974). Cerebrocerebellar communication systems. In *Physiological Reviews*. https://doi.org/10.1152/physrev.1974.54.4.957

Binzegger, T., Douglas, R. J., & Martin, K. A. C. (2004). A quantitative map of the circuit of cat primary visual cortex. *Journal of Neuroscience*. https://doi.org/10.1523/JNEUROSCI.1400-04.2004

Hooks, B. M., Mao, T., Gutnisky, D. A., Yamawaki, N., Svoboda, K., & Shepherd, G. M. G. (2013). Organization of cortical and thalamic input to pyramidal neurons in mouse motor cortex. *Journal of Neuroscience*. https://doi.org/10.1523/JNEUROSCI.4338-12.2013

Izhikevich, E. M. (2003). Simple model of spiking neurons. *IEEE Transactions on Neural Networks*, *14*(6), 1569–1572. https://doi.org/10.1109/TNN.2003.820440

Kar, K., & DiCarlo, J. J. (2020). Fast recurrent processing via ventral prefrontal cortex is needed by the primate ventral stream for robust core visual object recognition. *BioRxiv*. https://doi.org/10.1101/2020.05.10.086959

Mazzoni, A., Panzeri, S., Logothetis, N. K., & Brunel, N. (2008). Encoding of naturalistic stimuli by local field potential spectra in networks of excitatory and inhibitory neurons. *PLoS Computational Biology*, *4*(12). https://doi.org/10.1371/journal.pcbi.1000239

Papale, A. E., & Hooks, B. M. (2018). Circuit changes in motor cortex during motor skill learning. In *Neuroscience*. https://doi.org/10.1016/j.neuroscience.2017.09.010

Phillips, J. W., Schulmann, A., Hara, E., Winnubst, J., Liu, C., Valakh, V., Wang, L., Shields, B. C., Korff, W., Chandrashekar, J., Lemire, A. L., Mensh, B., Dudman, J. T., Nelson, S. B., & Hantman, A. W. (2019). A repeated molecular architecture across thalamic pathways. *Nature Neuroscience*. https://doi.org/10.1038/s41593-019-0483-3

Rongala, U. B., Spanne, A., Mazzoni, A., Bengtsson, F., Oddo, C. M., & Jörntell, H. (2018). Intracellular dynamics in cuneate nucleus neurons support self-stabilizing learning of generalizable tactile representations. *Frontiers in Cellular Neuroscience*. https://doi.org/10.3389/fncel.2018.00210

Spanne, A., Geborek, P., Bengtsson, F., & Jörntell, H. (2014). Spike generation estimated from stationary spike trains in a variety of neurons In vivo. *Frontiers in Cellular Neuroscience*. https://doi.org/10.3389/fncel.2014.00199

Yamawaki, N., Borges, K., Suter, B. A., Harris, K. D., & Shepherd, G. M. G. (2014). A genuine layer 4 in motor cortex with prototypical synaptic circuit connectivity. *ELife*. https://doi.org/10.7554/eLife.05422

| A | B | C | a | b | c | d |
|---|---|---|---|---|---|---|
| 0.04 | 5 | 140 | 0.02 | 0.2 | -65 | 8 |

**Table 1.** Izhikevich neuron model parameters used in the evaluation of this study.

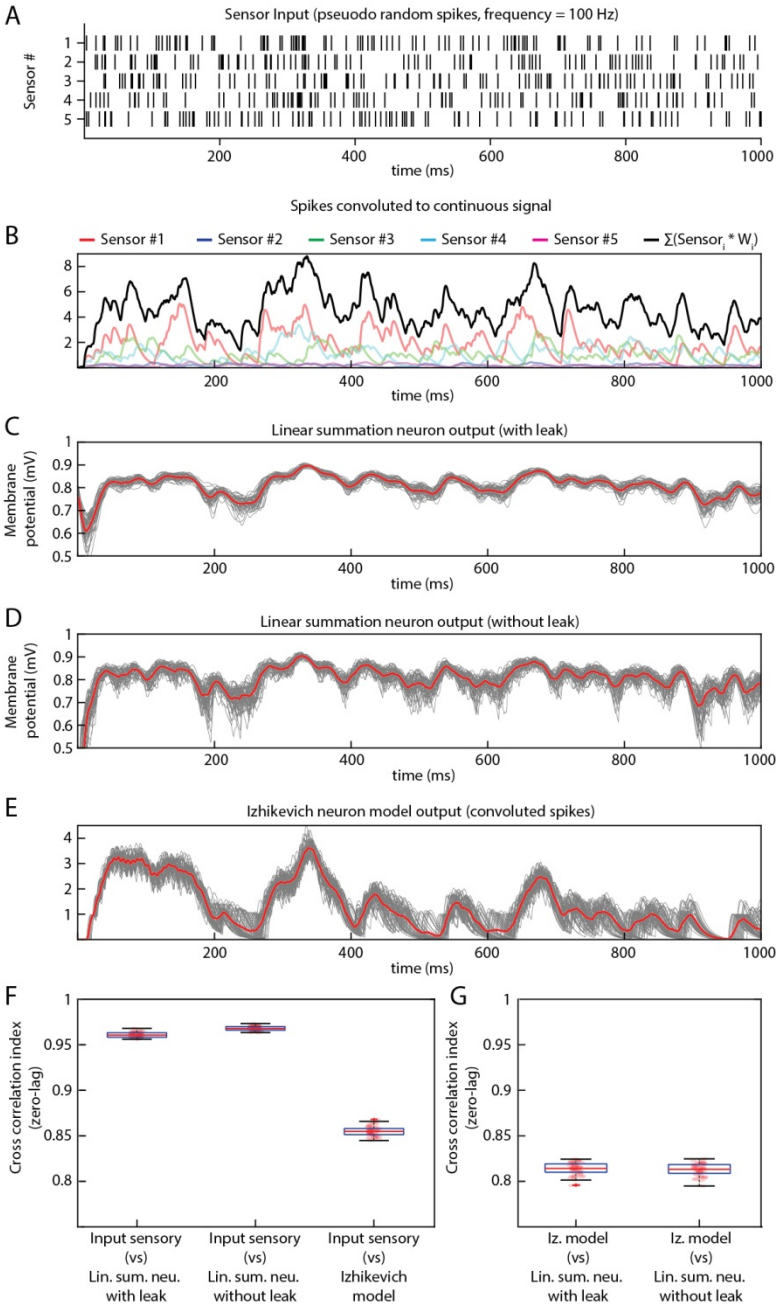


**Figure 1**: Neuron model comparison. **(A)** Pseudo-random input spike trains (5 spike trains illustrating 5 sensory inputs) **(B)** The input spike trains convoluted using a kernel function (see Methods). The convoluted input responses were fed as weighted (randomly generated) EPSP inputs to the neuron model. We add a gaussian noise (sigma = 10 ms) to these input spike trains, to attain 50 repetitions of the input. The input spike frequency is 100 Hz for this analysis. (**C**) LIS neuron model output without dynamic leak. The red line is the mean across 50 responses (corresponding to 50 input repetitions, black lines). (**D**) LIS neuron model output with dynamic leak. (**E**) Izhikevich neuron model output. The output spikes of the Izhikevich neuron model were convoluted using kernel function (with similar time constants of input spike convolution). (**F**) Cross-correlation measure between the sensory input and output responses of LIS model (with and without dynamic leak) and Izhikevich neuron

model. (**G**) Cross-correlation measure between the output response of LIS model responses (with and without dynamic leak) and Izhikevich neuron model.

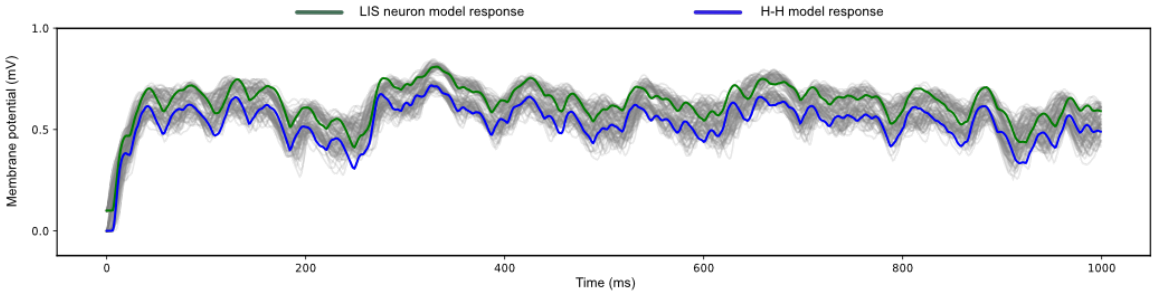


**Supplementary Figure 1**: Neuron model. A compassion between the output responses for LIS neuron model (green line) and the H-H derived backward Euler model (blue line), for a given pseudo-random spike inputs (as discussed in Figure 1A, B). The responses of LIS neuron model output were offset by 0.1 mV, in order to visualize the coherence between the both neuron model responses.

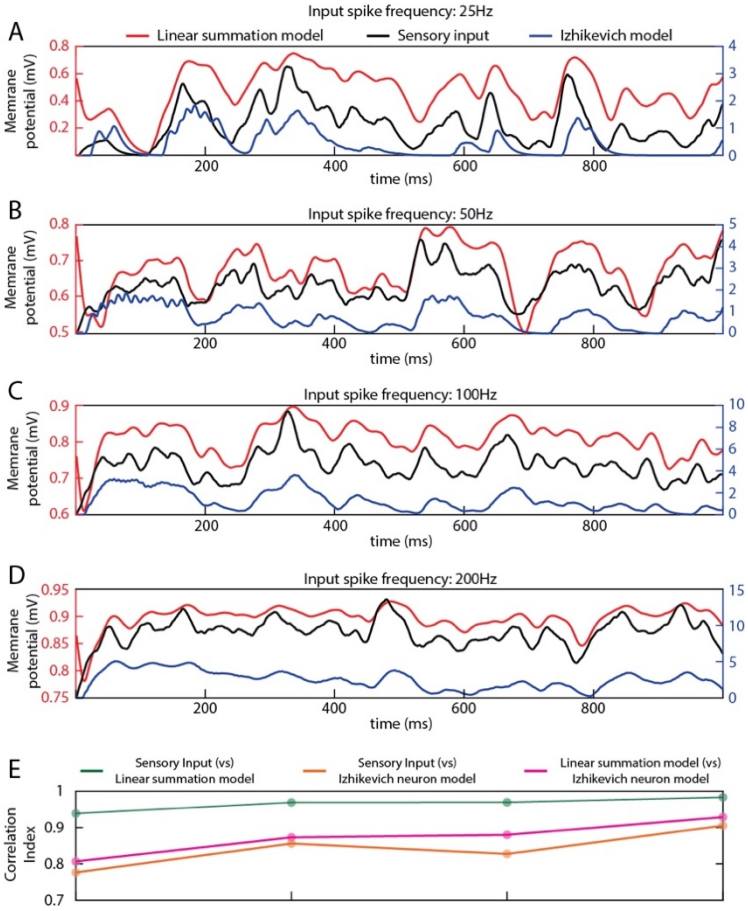


**Supplementary Figure 2**: Neuron model (LIS & IZ) output comparison for different input spike frequencies. (**A-D**) Neuron responses for LIS model (with leak) and IZ neuron model, based on different input spike frequencies. (**E**) Cross-correlation measure between sensory inputs and the neuron models (LIS and IZ) respective output.

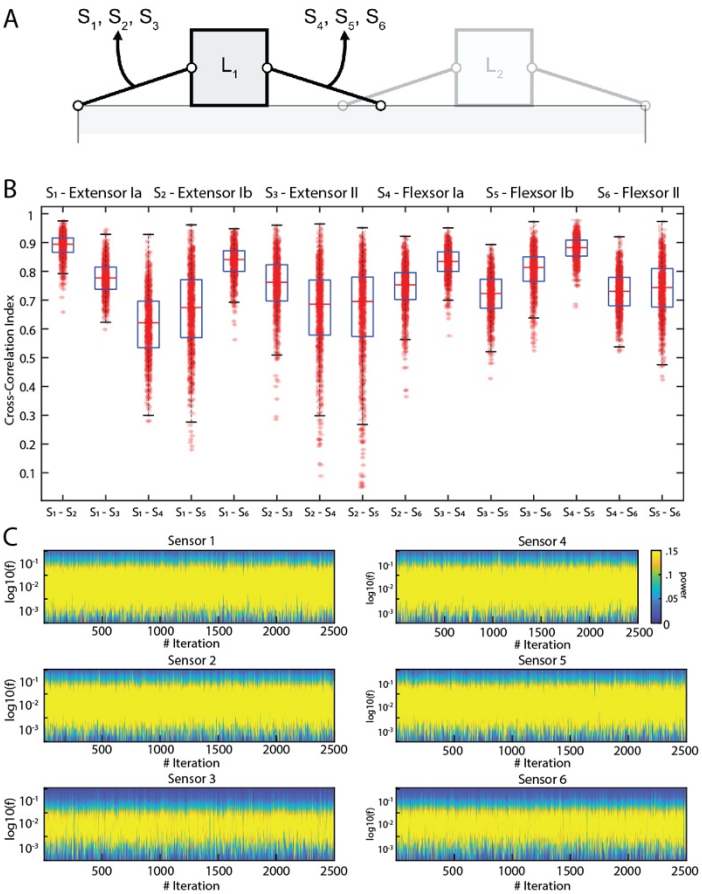


**Figure 2**: Properties of the pseudoreal sensory data used to drive the activity of the simulated neuronal network: (**A**) A model plant was created with a link (L1) resting on a plane with a sliding constraint. A pair of antagonistic joints (J1, J2) was attached to L1. (**B**) Cross-correlation analysis between the six synthesized sensory signals. (**C**) Time-continuous frequency power analysis for all the 6 sensory responses across 2500 iterations.

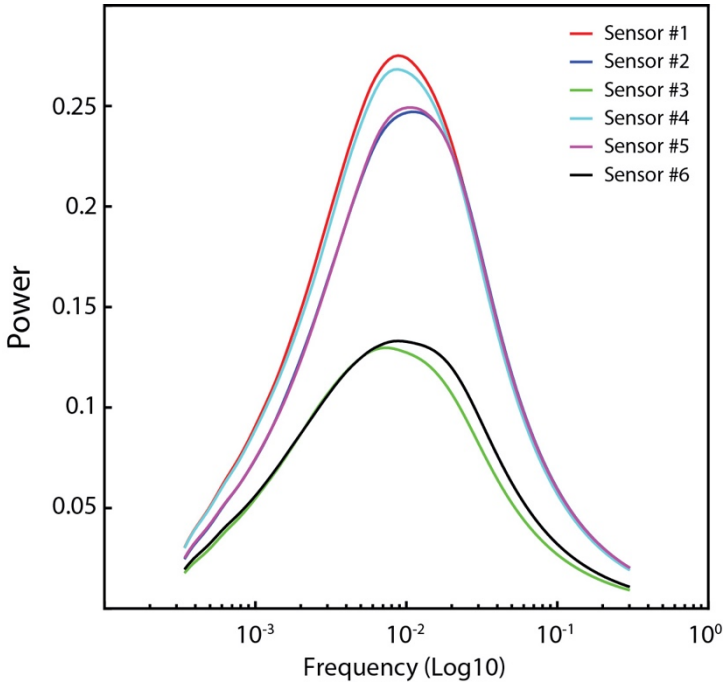


**Supplementary Figure 3**: An average of time-continuous frequency power analysis, for 500 iteration cycles (Iteration #500-1000) across all the 6 sensors.

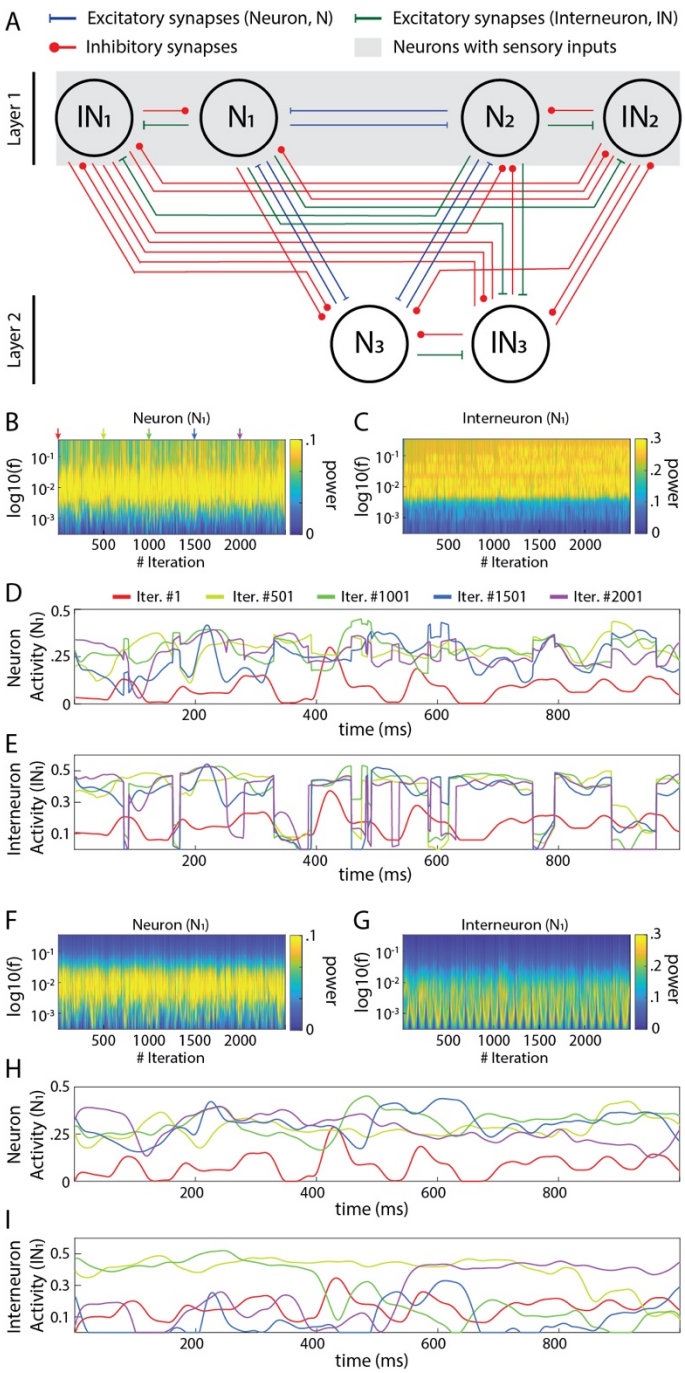


**Figure 3:** Network architecture and examples of frequency power plots at different iterations of the network simulation. (**A**) Principles of the connectivity structure in the recurrent network studied. Note that the default network contained excitatory neurons (5 in the input layer, 4 in the output layer) and inhibitory neurons (same numbers) with the same connectivity. (**B**) Frequency power plot of the activity in an excitatory neuron. (**C**) Similar plot for an inhibitory neuron. (**D**) Raw data plots for sample signals in the excitatory neuron generated at the indicated iteration. (**E**) Similar plot for the inhibitory neuron. (**F**)-(**I**) Similar plots as in (**B**)-(**E**) but when all the neurons were modelled to include the dynamic leak.

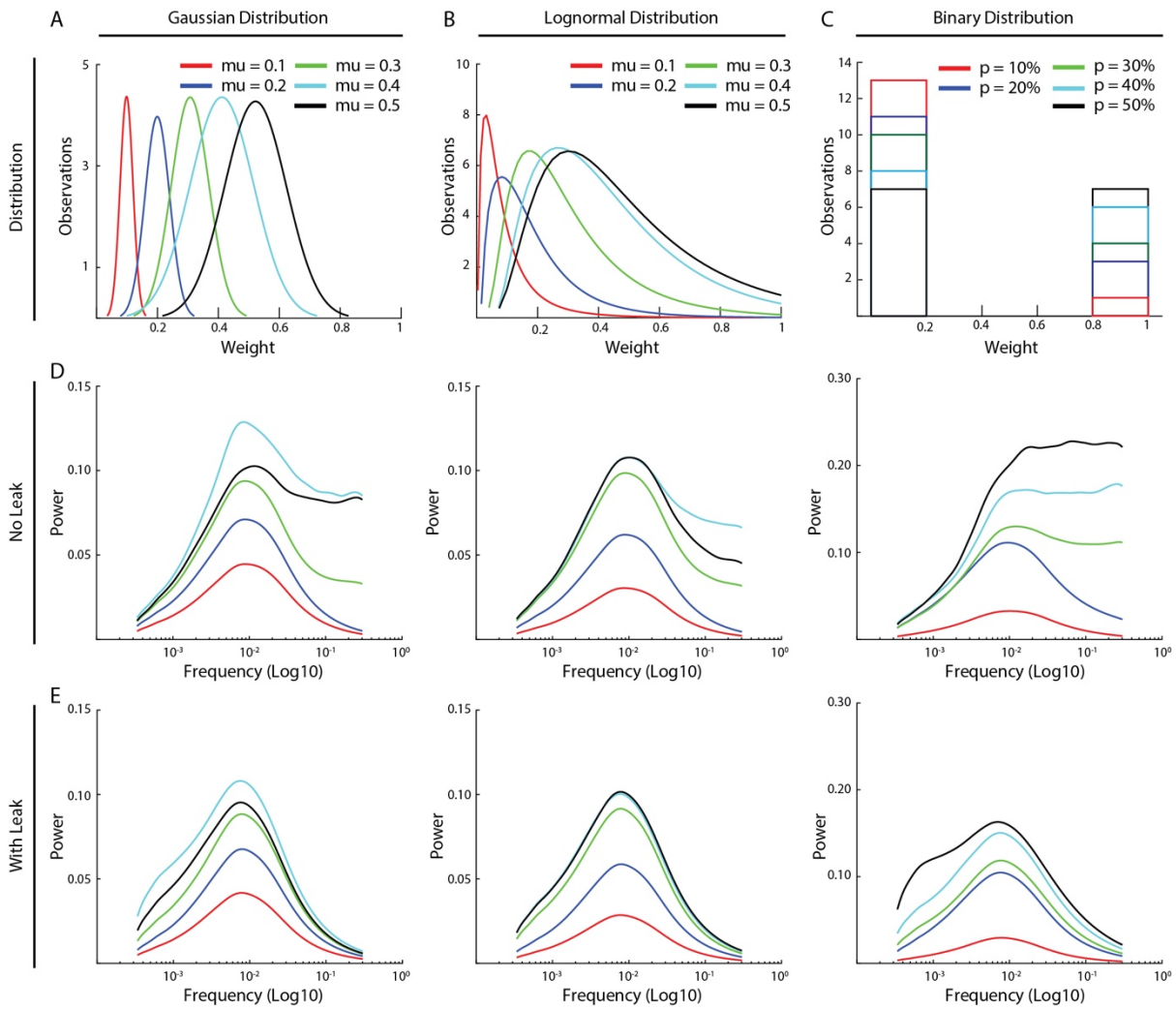


**Figure 4:** The appearance of high-frequency components was independent of the type of synaptic weight distribution and was always cancelled by dynamic leak. (**A-C**) The three types of synaptic weight distributions explored, Gaussian, Log-Normal and Binary, and there shape for five different mean connectivity strengths. (**D**) The high frequency components produced in the recurrent networks with different mean connectivity strength (color keys in A-C) across the three types of synaptic weight distributions. (**E**) Similar display as in C but for neuron model with dynamic leak.

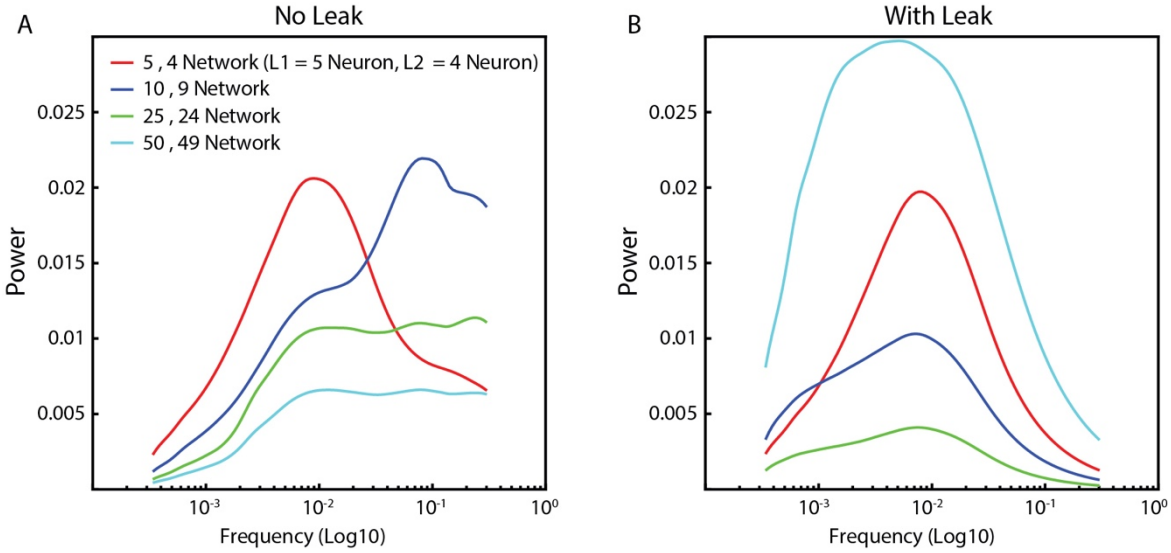


**Figure 5:** (A) The high frequency components appeared regardless of network size. (B) Introduction of dynamic leak 'rescued' the network from these high-frequency components.

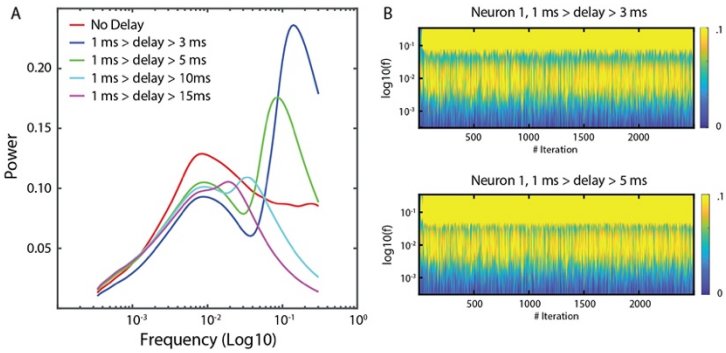


**Figure 6: Neuronal conduction delays.** (**A**) High frequency components were worsened by adding neuronal delays (3ms, 5ms). Further increase in the neuronal delays (10ms, 15ms) alters the underlying activity signal, which can be perceived from multiple power peaks. (**B**) Frequency power plot of the activity in an excitatory neuron (N1), for neuronal delays of 3ms and 5ms.